Redox Reaction Characteristics of Ferritin Immobilized onto Poly(L-lysine)-Modified Indium Oxide Electrodes

Masato Tominaga*, Kazuki Soejima, and Isao Taniguchi*

Graduate School of Science and Technology,

Kumamoto University, Kumamoto 860-8555, Japan

*Corresponding author

Graduate School of Science and Technology,

Kumamoto University,

e-mail: masato@gpo.kumamoto-u.ac.jp

Tel.: +81-96-342-3656, Fax: +81-96-342-3656

Abstract

Ferritin-immobilized poly(L-lysine)-modified electrodes showed well-defined redox waves representing ferritin. Cathodic and anodic peak currents obtained from cyclic voltammograms were proportional to potential sweep rates. From charge flow values during oxidation or reduction reactions calculated by peak areas in cyclic voltammograms, and the surface coverage of ferritin, reacted iron atoms per ferritin molecule were calculated. Obtained numbers of reacted iron atoms were significantly smaller than expected values from iron atoms at ferrihydrite core surfaces of ferritin, which would be caused by the rate-determining ion flow through ion channels of ferritin to compensate for charges in the ferritin cavity. Anodic and cathodic peak potentials in cyclic voltammograms were significantly dependent on cationic species in the solution, though voltammetric shapes and peak currents were independent of cations. From the obtained results that structural changes in ferritin were not detected by fluorescent spectra, it is thought that the cationic dependence on ferritin redox peak potentials is caused by ferritin cores.

Keywords: ferritin; redox reaction; modified electrode; potential; indium oxide

1. Introduction

Ferritins provide a means for living systems to gain access to essential mineral nutrients under conditions that otherwise favor the formation of hydrous ferric oxide, a biologically inert form of iron. Ferritins consist of protein shells formed from highly symmetrical subunits and from mineral cores containing up to *ca.* 4500 iron atoms in the form of ferrihydrite phosphate, $(FeOOH)_8(FeOPO_3H_2)$ [1-9]. The outside diameter of the shell is *ca*. 12 nm, and the cage that surrounds a hollow cavity is roughly 8 nm in diameter. Eight hydrophilic 3-fold channels and six hydrophobic 4-fold channels surround the shell, which provides access to the protein interior, presumably for electrons, protons, small ions and molecules. 3-fold channels are proposed as the main entry route for iron [1-9]. Iron uptake and release mechanisms are caused by iron (Fe(III) / Fe(II)) redox reactions [1-9]. In view of the interesting properties of ferritin, this protein has been studied extensively with regards to biochemistry [1-11] as well as in the protein engineering of viral cages for constrained nano-material syntheses [12-17].

Direct electron transfer reactions of ferritin at electrodes were recently reported [18-25]. The electrochemistry of ferritin adsorbed onto tin-doped indium oxide and bare gold electrode surfaces due to hydrophobic interactions in highly ionic solutions was investigated [19-22]. We reported ferritin-immobilized electrodes based on self-assembled monolayer (SAM)-modified gold electrodes, using electrostatic interactions between ferritin and terminal SAM functional groups [24,25]. Furthermore, recently we demonstrated direct electron transfer reaction of ferritin immobilized onto polypeptide-functionalized indium oxide electrodes using electrostatic interactions between polypeptides and ferritin [26]. As described above, iron uptake and release of ferritin is caused by oxidation and reduction reactions of iron ions in ferritin shell. Thus, before the observation of direct electron transfer of ferritin, the behaviors of iron uptake and release of ferritin were investigated using oxidant and reductant reagents [1-9]. Electrochemistry of ferritin has possibility for easily and precision control of the iron uptake and release of ferritin. To analyze the

ferritin function by electrochemisty, we should have knowledge for electrochemical redox reaction characteristics of ferritin. In the present study, we used ferritin-immobilized poly(L-lysine)-modified electrodes, to evaluate and analyze anodic and cathodic peak currents, and peak potentials. The preliminary results suggest that peak currents in cyclic voltammograms are governed by a rate-determining ion flow through ferritin ion channels to compensate for charges in the ferritin cavity. Furthermore, anodic and cathodic peak potentials in cyclic voltammograms were significantly dependent on cationic species.

2 Experimental

2.1. Ferritin and materials

Horse spleen ferritin (from Sigma) was purified by size exclusion chromatography [6]. The concentration of purified ferritin was determined by measuring its absorbance at 562 nm, followed by BCA-protein reactions (BCA protein assay kit, Pierce Chem. Comp.) against an albumin standard curve [27]. The number of iron atoms per ferritin molecule used in this study was determined to be 3×10^3 atoms by inductively coupled plasma-atomic emission spectroscopy (ICP-AES) using the IRIS Advantage (Jarrell-Ash Co.) and atomic absorption spectroscopy using a Nippon Jarrell Ash AA-845 Atomic Absorption & Flame Emission Spectrophotometer. Poly-(L-lysine) (PLL, molecular weight: 93,800 Da) was obtained from Sigma, and used as received. Water was purified with a Millipore Milli-Q water system. Other reagents were of analytical grade.

2.2. Preparation of ferritin-immobilized poly-(L-lysine)-modified indium oxide electrode

Ferritin-immobilized poly-(L-lysine)-modified electrodes (ferritin-PLL-modified electrode) were prepared according to previous reports [26]. Briefly, an indium oxide electrode (Kinoene Optics Corp., Japan, or Kuramoto Corp., Japan, geometric area: 0.25 cm^2) was used as a working electrode. The electrode was cleansed by ultra sonication in a 1% aqueous New-Vista (AIC Corp.)

solution according to methods described elsewhere [28]. PLL-modified electrodes were obtained by immersing indium oxide electrodes into phosphate buffer solutions (ionic strength, $\mu = 0.1$, pH 7.0) in the presence of 1 mg ml^{-1} PLL for 30 min. In neutral solutions, positively charged PLL adsorbed on negatively charged indium oxide electrode surfaces by electrostatic interactions [29]. The PLL-modified indium oxide electrode was immersed into phosphate buffer solution with 2 μmol dm^{-3} ferritin for 60 min. Then, electrodes were rinsed with buffer solution and transferred to buffer solution devoid of ferritin.

2.3. Instrumentation

Fluorescence spectra were recorded with a Spectrofluorometer FP-6500, JASCO. A multimode NanoScope III (Digital Instruments) was utilized for tapping-mode atomic force microscopic (AFM) imaging. Standard phosphorus doped silicon cantilevers were used. The calibration was performed by imaging standard grating samples. Tapping-mode AFM measurements were carried out under an air atmosphere.

Electrochemical measurements were carried out in a phosphate buffer solution under a nitrogen atmosphere using a Potentiostat PS-6, Toho Giken Corp., Japan, with a function generator. An Ag/AgCl (saturated KCl) electrode and a Pt plate were used as reference and auxiliary electrodes, respectively. All potentials are reported with respect to an Ag/AgCl (saturated KCl) electrode. Prior to cyclic voltammetric measurements, a phosphate buffer solution ($\mu = 0.1$, pH 7.0) was de-aerated with high purity argon gas, and a positive pressure of argon gas was maintained over the solution during all electrochemical experiments.

3. Results and Discussion

3.1. Electrode reactions at ferritin-PLL-modified indium oxide electrode

Fig. 1 shows the surface morphology of a polished indium oxide (from Kuramoto Corp., Japan), a PLL-modified indium oxide and a ferritin-immobilized PLL-modified indium oxide electrode surfaces by tapping-mode AFM measurements. The indium oxide and PLL-modified electrode surfaces were flat at an atomic level. After electrodes were modified with ferritin, monolayers of ferritin molecules adsorbed onto surfaces. The size of each ferritin molecule was evaluated to be approximately 11 (± 1.5) nm in diameter, which was comparable to the expected ~12 nm diameter determined by x-ray diffraction [1-9]. These results ae similar to our previously reported results [26].

Fig. 2 shows typical cyclic voltammograms in phosphate buffer solutions (μ = 0.1, pH 7.0) at various potential sweep rates, after PLL-modified indium oxide electrodes were immersed into a phosphate buffer solution of 2 μmol dm^{-3} ferritin for 60 min. Well-defined redox waves representing ferritin were observed. Oxidation and reduction peaks were observed around –0.10 and –0.22 V, respectively, at a potential sweep rate of 50 mV s^{-1}. A redox response for ferritin was not observed in the buffer solution, when indium oxide and PLL-modified electrodes were used. Fig. 3 shows plots of cathodic and anodic peak currents in cyclic voltammograms from ferritin-PLL-modified electrode as a function of potential sweep rates. Voltammograms at various potential sweep rates were obtained from individual ferritin-PLL-modified electrodes. Both cathodic and anodic peak currents were proportional to potential sweep rates at a sweep range of 20 to 200 mV s^{-1}. Herein, the redox reaction of ferritin can be roughly understood as follows: Fe(III) atoms, which consists of ferrihydrite cores of ferritin, sited around core surfaces reduce to Fe(II) atoms during negative potential sweeps in voltammograms. From the aforementioned reaction, it was expected that the electrode reaction behaviors show the adsorbed species reaction type. In fact, the cathodic peak current increased linearly with an increasing potential sweep rate. Reduced Fe(II) atoms would still site at the same position at the core surface, or release from the core surface, as shown in Fig. 4, because the solubility of Fe(II) ($(Fe(OH)_2$: $K_{sp} \approx 10^{-15}$ (mol $dm^{-3})^2$) is much

higher than that of Fe(III) ((Fe(OH)$_3$: $K_{sp} \approx 10^{-39}$ (mol dm^{-3})^3) under physiological pH [30]. Thus, during positive potential sweep, it is expected that the electrode reaction behaviors would show the diffusion-controlled electrode reaction type, or reaction type mixed with diffusion-controlled and adsorbed species reaction types. However, the obtained results showed a linearly relationship between anodic peak currents and potential sweep rates. The difference between expectation and obtained results could be understood by thin-layer electrochemical behavior. The following equation (1) shows the relation between the root-mean-

$$x^2 = 2Dt \qquad (1)$$

square displacement, x^2, at time t and the diffusion coefficient, D. Assuming D and t are 1×10^{-5} cm^2 s^{-1} and 14 seconds (sweep time from 200 to -500 mV at a scan rate of 50 mV s^{-1}), the resulting estimated finite diffusion layer is calculated to be 1.7×10^{-2} cm. This obtained finite diffusion layer is significantly larger than the ferritin cavity (*ca*. 8 nm in diameter). Considering the nanospace of the ferritin cavity is *ca.* 8 nm in diameter ($x = 8 \times 10^{-7}$ cm), the finite diffusion layer would react at *ca*. 3×10^{-8} s. Thus, within the cyclic voltammetric time scale of this study, linear relationships between anodic peak currents and potential sweep rates were observed.

From the linear relationship between peak currents and potential sweep rates in potential sweep rates of 20 to 200 mV s^{-1}, values of charge flow (C cm^{-2}) during oxidation or reduction reactions were calculated by the peak areas from cyclic voltammograms. During the first cycle of voltammmetric measurements, charge flow values of reduction and oxidation processes in cathodic and anodic peaks were evaluated to be 7.4×10^{-6} and 5.0×10^{-6} C cm^{-2}, respectively, indicating that 7.7×10^{-11} mol cm^{-2} Fe(III) and 5.2×10^{-11} mol cm^{-2} Fe(II) (4.6×10^{13} ions cm^{-2} Fe(III) and 3.1×10^{13} ions cm^{-2} Fe(II)) had reacted. In a previous report, we reported that the surface coverage of ferritin immobilized onto a PLL-modified electrode was $9\sim13 \times 10^{11}$ molecules cm^{-2}. Using this

surface coverage value for ferritin, 43 (± 8) ions per ferritin molecules Fe(III) were reduced and 29 (± 5) ions per ferritin molecules Fe(II) were oxidied. The evaluated results for numbers of reacted iron atoms provide two pieces of evidence. First, numbers of reacted iron atoms in ferritin cavity during reduction and oxidation reactions were significantly smaller than expected values from iron atoms at ferritin core surfaces. On redox reactions of iron atoms at ferritin core surfaces in ferritin cavity, the total charge in the cavity would be change. For example, before redox reaction of ferritin, total charge in ferritin cavity is maintained to be neutral. On the other hand, when ferritin core would be reduced, the total charge in ferritin cavity would change to positive. In order to compensate for change of charge in the ferritin cavity, in the other words, to keep electroneutrality in the cavity, ion (anions and/or cations) uptake and/or release passing through the ion channels of ferritin would occur (Fig. 4). This compensating ion uptake and/or release would be the rate-determining factor, thus the number of iron atoms actually related to redox reactions would be significantly smaller than that expected. In a previous report, kinetics of iron release from ferritin in 0.1 mol dm^{-3} Tris-HCl buffer (pH 7.4) solution was investigated by UV-visible spectroscopy using dihydroriboflavin as a reductant, and it was resulted that the maximum rate of iron release for horse spleen ferritin was evaluated to be 1.0 Fe(II) leaving per second per channel [30]. Roughly analyses in our case study, 43 (± 8) Fe(III) ions per feritin molecules were reduced during 14 seconds for reduction potential sweep in voltammetry. Thus, it is evaluated to be, roughly, 3 (± 0.5) Fe(III) ions per second per ferritin molecule would be reduced, and then the reduced 0.4 Fe(II) ions per second per channel might be released, because ferritin has eight 3-fold channels per molecule for iron ions passing. The obtained rate value of iron release is approximately half value with respect to the reported value. The difference results might be caused by follows: In the previous report, rate kinetics was studied using ferritin aqueous solution. On the other hand, in our study, ferritin molecules were adsorbed on PLL-modified electrode surface. Thus, some ion channels of ferritin molecule would be inaccessible, because the molecule would be covered with

PLL at the electrode surface. Second, the number of re-oxidized Fe(III) ions from Fe(II) ions was *ca.* two-third times the number of reduced Fe(II) ions from Fe(III) iron ions, which indicates that part of the reduced iron ions would be released from the ferritin cavity. This prediction is also supported by the fact that redox peaks gradually decreased during the potential cycling and were eventually not observed.

3.2. Anionic and cationic effects on redox reactions at ferritin-PLL-modified indium oxide electrodes

Anionic and cationic effects on the redox reactions of ferritin were investigated using various anionic and cationic species. Fig. 5a-c shows a redox reaction of ferritin-PLL-modified electrode in the presence of 300 mmol dm^{-3} NaCl, NaBr and NaI. Voltammetric shapes and peak currents were almost independent of the anionic species. Anodic and cathodic peak potentials are summarized in Table 1a, which indicate that peak potentials were almost independent of the anions. Fig. 5b,d,e shows the redox reaction of ferritin in the presence of NaBr, LiBr and KBr. Voltammetric shapes and peak currents were also independent of the cationic species. On the other hand, anodic and cathodic peak potentials were significantly dependent on the cationic species, as shown in Table 1b. Furthermore, we investigated peak potentials in the presence of LiCl, NaCl and KCl, as summarized in Fig. 6a,b. A tendency towards positive shifts in anodic and cathodic peak potentials with decreasing cation diameters (K < Na < Li) was observed.

To clarify whether the cation dependence on redox peak potentials was due to structural changes in ferritin or ferritin cores, we measured fluorescent spectra of ferritin in the presence of a cation. When ferritin was excited at 280 nm, it showed a fluorescence emission peak around 325 nm corresponding to tryptophan residues [31-33]. The peak position and intensity were almost independent of the cationic species, indicating that ferritin structural changes were not induced. In conclusion, these facts suggest that the cationic dependence of redox peak potentials of ferritin is

caused by ferritin cores, and does not arise because of structural changes. However, we cannot discuss this phenomenon in more detail, because electron transfers in ferritin remain unclear. The putative distance for electron transfers between ferrihydorite ferritin cores and an electrode surfaces is the thickness of the protein shell of *ca*. 2 nm, which is larger than that for long-range electron transfers observed in protein [34]. R. C. Davis and coworkers concluded, from conductive probe (CP) AFM measurements, that ferritin protein shells act as significant tunneling barriers for electron transfers [35]. Thus, it is expected that bound iron ions at positions around ion channels and/or on the inner faces of ferritin cavity, could act as an electron transfer mediator and accelerate electrons through the protein shells [36]. On the other hand, D. N. Axford and J. J. Davis used CP-AFM measurements to suggest the presence of direct tunneling electron transfers across protein layers [37].

4. Conclusions

In conclusion, ferritin molecules covered the whole surface of PLL-modified indium oxide electrodes were observed by AFM measurements using atomically flat electrodes. Ferritin-PLL-modified electrodes showed well-defined redox waves representing ferritin. Observed cathodic and anodic peak currents in cyclic voltammograms were proportional to potential sweep rates, and these aforementioned behaviors can be understood when considering the thin-layer electrochemistry of the nanospace of the ferritin cavity. From charge flow values during oxidation or reduction reactions calculated by peak areas in cyclic voltammograms, reacted Fe(III) and Fe(II) atoms during reduction and oxidation processes were evaluated to be 7.7×10^{-11} and 5.2×10^{-11} mol cm^{-2} (4.6×10^{13} and 3.1×10^{13} ions cm^{-2}), respectively. Using the surface coverage of ferritin ($9\sim13 \times 10^{11}$ molecules cm^{-2}), 43 ($\pm$ 8) ions per ferritin molecules Fe(III) were reduced and 29 ($\pm$ 5) ions per ferritin molecules Fe(II) were oxidized. Anodic and cathodic peak potentials in cyclic voltammograms were significantly dependent on cationic species in solutions, even though

voltammetric shapes and peak currents were independent of these species. Positive shift tendencies in anodic and cathodic peak potentials with decreasing diameters of cations were observed. Since structural changes in ferritin were not detected in fluorescent spectra, it is thought that the cationic dependence on redox peak potentials of ferritin is caused by ferritin core.

Although ferritin redox reaction details remain unclear, the results presented herein are useful in understanding the physiology of ferritin, and they demonstrate how electrochemical methods are useful in characterizing ferritin functions.

Acknowledgment

This work was supported by a Grant-in-Aid for Scientific Research (MT) from the Ministry of Education, Culture, Science, Sports and Technology, Japan.

References

[1] P.M. Harrison, T.H. Lille, in: T.M. Loehr (Ed.), Iron Carriers and Iron Proteins, VCH Press, New York, 1989.

[2] T.G. St. Pierre, P. Chan, K.R. Bauchspiess, J. Webb, S. Betteridge, S. Walton, D.P.E. Dickson, Coord. Chem. Rev. 151 (1996) 125.

[3] P.M. Proulx-Curry, N.D. Chasteen, Coord. Chem. Rev. 144 (1995) 347.

[4] P. M. Harrison, P. Arosio, Biochim. Biophys. Acta 1275 (1996) 161.

[5] P. Arosio, T.G. Adellman, J.W. Drysdale, J. Biol. Chem. 253 (1978) 4451.

[6] G.D. Watt, R.B. Frankel, G.C. Papaefthymiou, Proc. Natl. Acad. Sci. 82 (1985) 3640.

[7] F.H.A. Kadir, F.K. Al-Massad, S.J.A. Fatemi, H.K. Singh, M.T. Willson, G.R. Moore, Biochem. J. 278 (1991) 817.

[8] R.K. Watt, R.B. Frankel, G.D. Watt, Biochemistry 31 (1992) 9673.

[9] X. Liu and E. C. Theil, Acc. Chem. Res. 38 (2005) 167.

[10] M. T. Klem, M. Young, T. Douglas, Materials Today 8 (2005) 28.

[11] Z. yang, X. Wang, H. Diao, J. Zhang, H. Li, H. Sun, Z. Guo, Chem. Commun. (2007) 3453.

[12] T. Douglas, V.T. Stark, Ionrg. Chem. 39 (2000) 1828.

[13] M. Allen, D. Willits, J. Mosolf, M. Young, T. Douglas, Adv. Mater. 14 (2002) 1562.

[14] J. M. Dominguez-Vera, E. Colacio, Inorg. Chem. 42 (2004) 6983.

[15] I. Yamashita, Thin Solid Films 393 (2001) 12.

[16] M. Tominaga, A. Ohira, A. Kubo, I. Taniguchi, M. Kunitake, Chem. Commun. (2004) 1518.

[17] I. Kim, H.-A. Hosein, D. R. Strongin, T. Douglas, Chem. Mat. 14 (2002) 4874.

[18] T.D. Martin, S.A. Monheit, R.J. Niichel, S.C. Peterson, C.H. Campbell, D.C. Zapien, J. Electroanal. Chem. 420 (1997) 279.

[19] R.J. Cherry, A.J. Bjornsen, D.C. Zapien, Langmuir 14 (1998) 1971.

[20] M.-S. Pyon, R.J. Cherry, A.J. Bjornsen, D.C. Zapien, Langmuir 15 (1999) 7040.

[21] D.C. Zapien, M.A. Johnson, J. Electroanal. Chem. 494 (2000) 114.

[22] F. Marken, D. Partel, C.E. Madden, R.C. Millward, S. Fletcher, New J. Chem. 26 (2002) 259.

[23] M. Tominaga, I. Taniguchi, Chem. Lett. 32 (2003) 954.

[24] M. Tominaga, I. Taniguchi, Chem. Lett. (2001) 704.

[25] M. Tominaga, A. Ohira, Y. Yamaguchi, M. Kunitake, J. Electroanal. Chem. 566 (2004) 323.

[26] M. Tominaga, K. Soejima, M. Matsumoto, I. Taniguchi, J. Electroanal. Chem. 579 (2005) 51.

[27] P.K. Smith, R.I. Krohn, G.T. Hermanson, A.K. Mallia, F.H. Gartner, M.D. Provenzano, E.K. Fujimoto, N.M. Goeke, B.J. Olson, D.C. Klenk, Anal. Biochem. 150 (1985) 76.

[28] M. Tominaga, T. Kumagai, S. Takita, I. Taniguchi, Chem. Lett. (1993) 1771.

[29] I. Taniguchi, Y. Hirakawa, K. Iwakiri, M. Tominaga, K. Nishiyama, J. Chem. Soc., Chem. Commun. (1994) 953.

[30] T. Jones, R. Spencer, C. Walsh, Biochem. 17 (1978) 4011.

[31] S. Stefanini, E. Chiancone, E. Antonini, FEBS Lett. 69 (1976) 90.

[32] S. Stefanini, E. Chiancone, P. Arosio, A. Finazzi-Agrb, E. Antonini, Biochem. 21 (1982) 2293.

[33] J. F. Collawn, Jr. H. Donato, Jr. W. W.Fish, Biochim. Biophys. Acta 871 (1986) 235.

[34] C. C. Page, C. C. Moser, X. Chen, P. L. Dutton, Nature 402 (1999) 47.

[35] D. Xu, G. D. Watt, J. N. Harb, R. C. Davis, Nano Lett. 5 (2005) 571.

[36] R. B. Frankel, G. C. Papaefthymiou, Hyperfine Interact. 33 (1987) 233.

[37] D. N. Axford, J. J. Davis, Nanotechnology 18 (2007) 1.

Figure Captions

Fig. 1. Tapping–mode AFM images of a polished indium oxide electrode surface (a), its surface modified with poly(L-lysine) (b) and a ferritin-immobilized poly(L-lysine)-modified electrode surface (c, d). The cross-sectional view corresponds to the line drawn (d).

Fig. 2. Typical cyclic voltammograms from ferritin-immobilized poly(L-lysine)-modified indium oxide electrodes in phosphate buffer solutions (pH 7). Potential sweep rates: 200, 150, 100, 50 and 20 mV s^{-1}. Electrode area: 0.25 cm^2.

Fig. 3. Plots of anodic (a) and cathodic (b) peak currents vs. potential sweep rates. Peak currents were obtained from cyclic voltammograms of ferritin-immobilized poly(L-lysine)-modified indium oxide electrodes in phosphate buffer solutions (pH 7). Electrode area: 0.25 cm^2.

Fig. 4. A schematic illustration of a ferritin redox reaction on the electrode surface and ion flow during the redox processes.

Fig. 5. Typical cyclic voltammograms from ferritin-immobilized poly(L-lysine)-modified indium oxide electrodes in phosphate buffer solutions (pH 6.5) in the presence of 300 mmol dm^{-3} NaCl (a), NaBr (b), NaI (c), LiBr (d) and KBr (e). Potential sweep rate: 50 mV s^{-1}. Electrode area: 0.25 cm^2.

Fig. 6. Cation effects on anodic (a) and cathodic (b) peak potentials of ferritin-immobilized poly(L-lysine)-indium oxide electrodes in phosphate buffer solutions (pH 6.5). Potential sweep rate: 50 mV s^{-1}.

Table1

Table 1a Effects of anion on anodic and cathodic peak potentials.

Electrolyte	Anodic peak potential / mV vs. Ag/AgCl	Cathodic peak potential / mV vs. Ag/AgCl
NaCl	-22.5	-217.5
NaBr	-25	-220
NaI	-35	-225

Table 1b Effects of cation on anodic and cathodic peak potentials.

Electrolyte	Anodic peak potential / mV vs. Ag/AgCl	Cathodic peak potential / mV vs. Ag/AgCl
LiBr	-7.5	-202.5
NaBr	-25	-220
KBr	-50	-240

The peak potential values were obtained from cyclic voltammograms of ferritin-immobilized poly(L-lysine)-modified indium oxide electrode in a phosphate buffer solution (pH 6.5) in the presence of 300 mmol dm^{-3} NaCl, NaBr, NaI, LiBr and KBr. Potential sweep rate: 50 mV s^{-1}. Electrode area: 0.25 cm^2.

Figure1

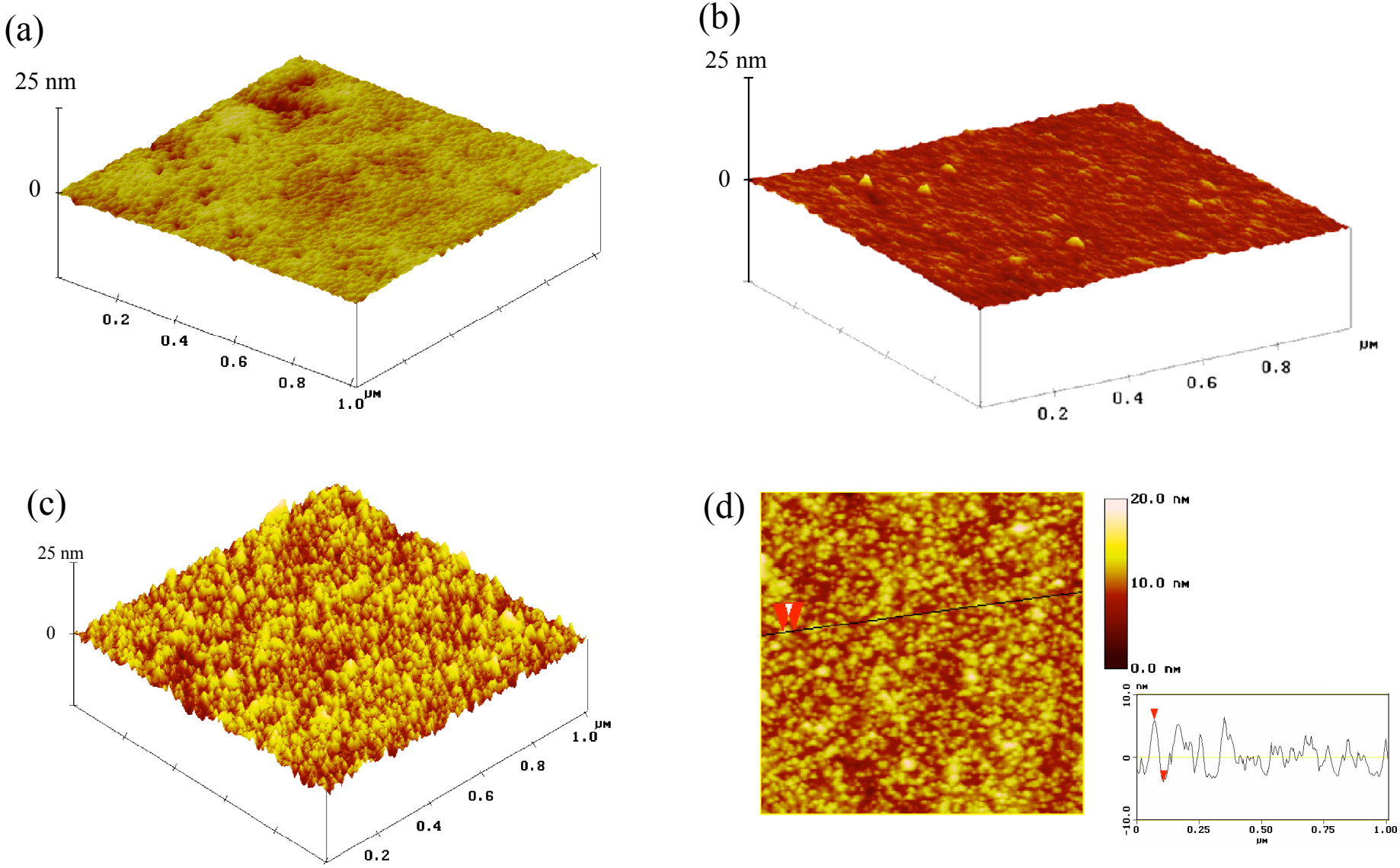

Fig. 1

Figure2

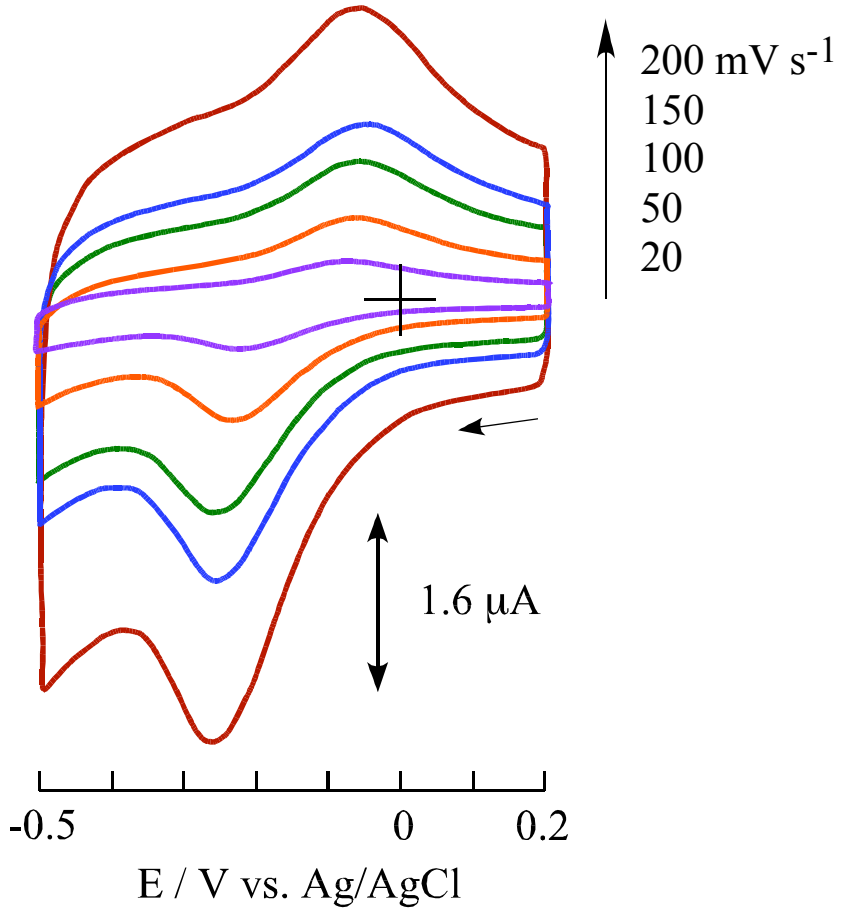

Fig. 2

Figure3

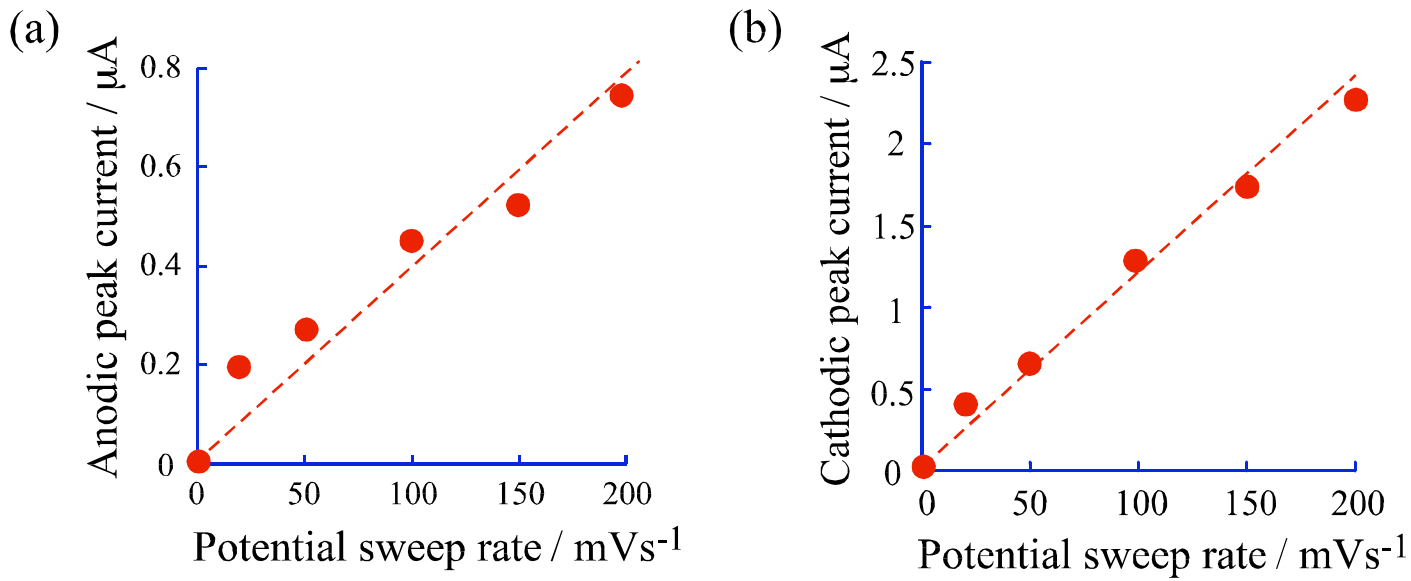

Fig. 3

Figure4

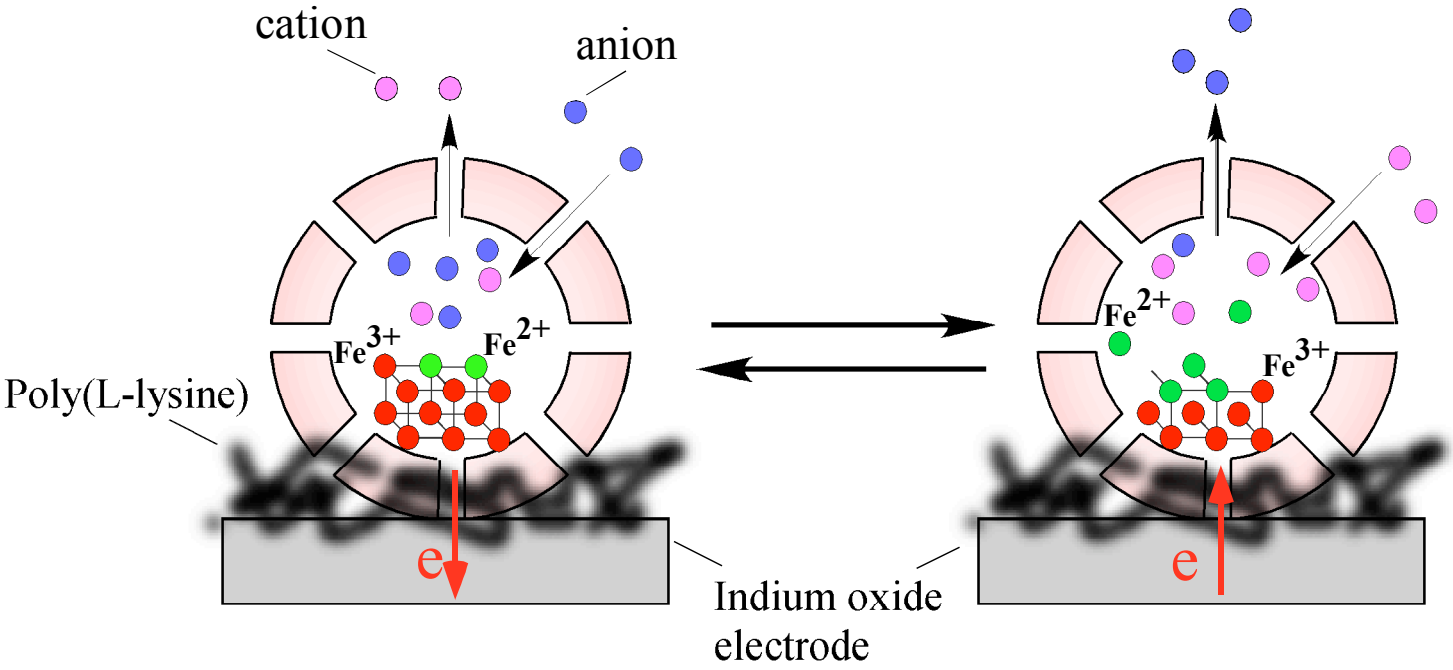

Fig. 4

Figure5

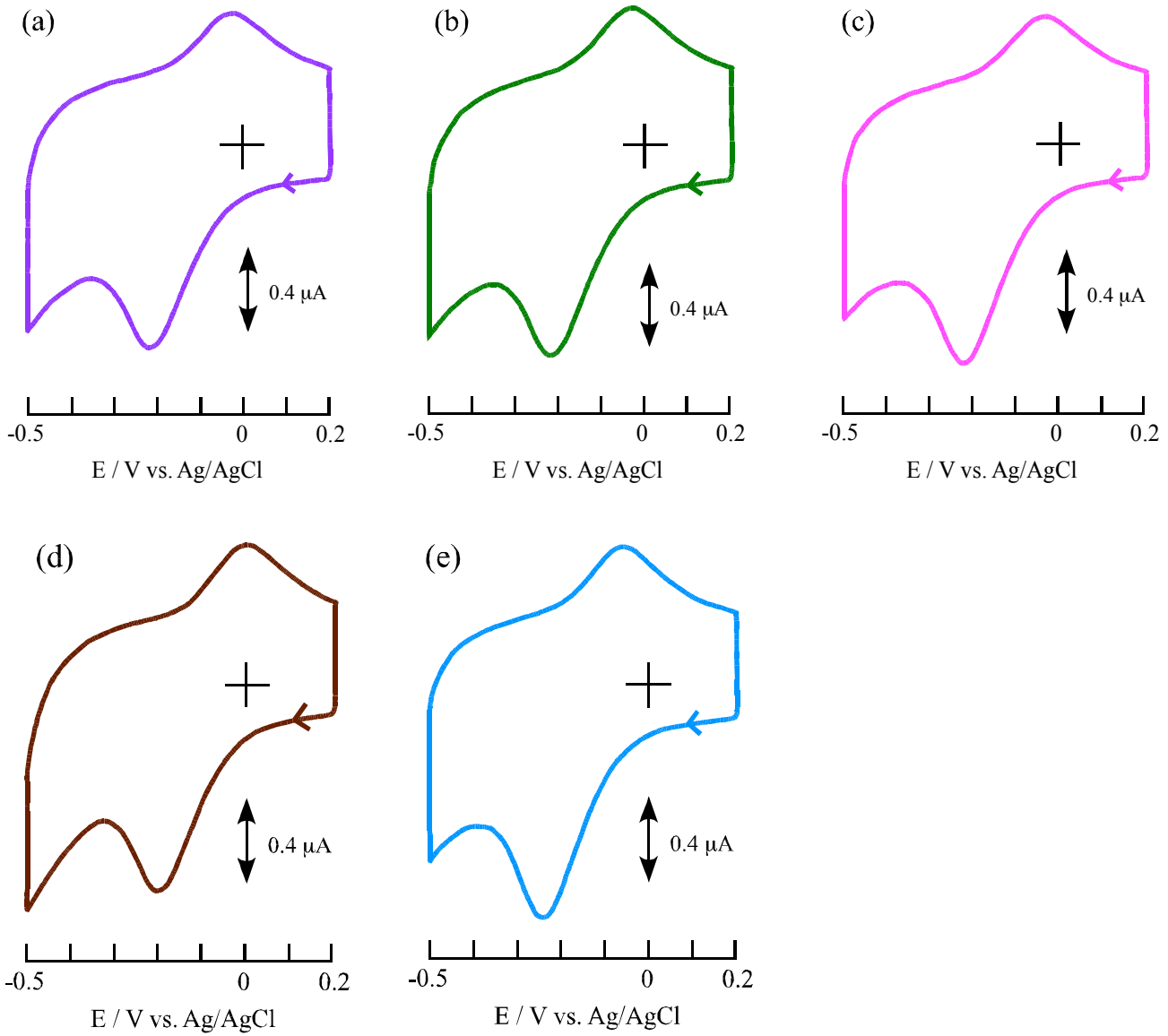

Fig. 5

Figure6

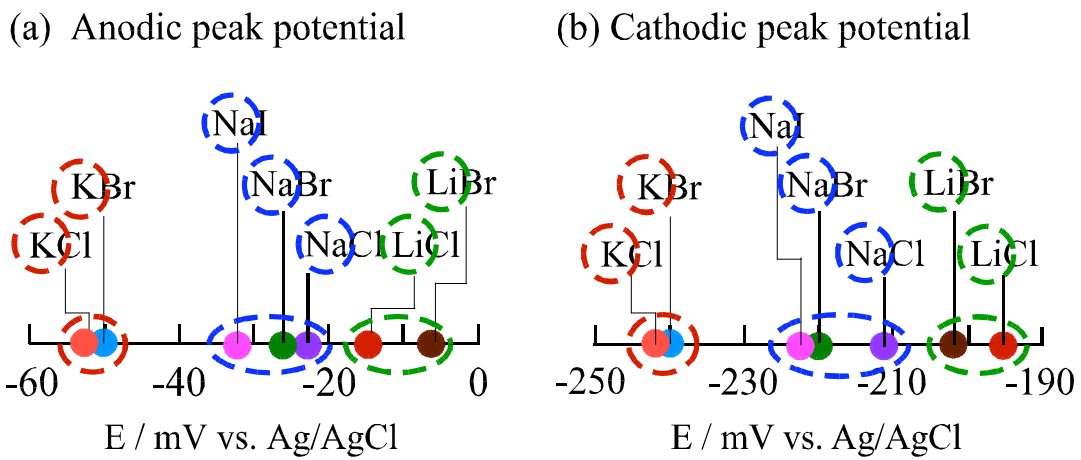

Fig. 6